

The AIMI Initiative: AI-Generated Annotations for Imaging Data Commons Collections

Gowtham Krishnan Murugesan¹, Diana McCrumb¹, Mariam Aboian², Tej Verma²,
Rahul Soni¹, Fatima Memon², Keyvan Farahani³, Linmin Pei⁴, Ulrike Wagner⁴,
Andrey Y. Fedorov⁵, David Clunie⁶, Stephen Moore¹, Jeff Van Oss¹

¹BAMF Health, Grand Rapids, MI, USA

²Yale School of Medicine, New Haven, CT, USA

³National Institute of Health, Bethesda, MD, USA

⁴Frederick National Laboratory for Cancer Research, Frederick, MD, USA

⁵Brigham and Women's Hospital and Harvard Medical School, Boston, MA, USA

⁶PixelMed Publishing, Bangor, PA, USA

Corresponding author: Gowtham Krishnan Murugesan (gowtham.murugesan@bamfhealth.com)

Abstract

The Image Data Commons (IDC) contains publicly available cancer radiology datasets that could be pertinent to the research and development of advanced imaging tools and algorithms. However, the full extent of its research capabilities is limited by the fact that these datasets have few, if any, annotations associated with them. Through this study with the Artificial Intelligence (AI) AI in Medical Imaging (AIMI) initiative, we produced high-quality, AI-generated imaging annotations of tissues, organs, and/or cancers for 11 distinct medical imaging collections from the IDC. These collections have a variety of image modalities, computed tomography (CT), magnetic resonance imaging (MRI), and positron emission tomography (PET) imaging modalities. Furthermore, the imaging collections cover various body parities, such as the chest, breast, kidneys, prostate, and liver. Both publicly available and novel AI algorithms were adopted and further developed using open-sourced data coupled with expert annotations to create the AI-generated annotations. A portion of the AI annotations were reviewed and corrected by a radiologist to assess the AI models' performances. Both the AI's and the radiologist's annotations conformed to DICOM standards for seamless integration into the IDC collections as third-party analyses. All the models and datasets (images and annotations) are publicly accessible.

Introduction

The National Cancer Institute (NCI) Imaging Data Commons (IDC) is a comprehensive repository of publicly available cancer imaging data, image-derived insights, and associated resources¹. These datasets, drawn from diverse public imaging initiatives such as The Cancer Imaging Archive (TCIA)², are standardized in the IDC according to the Digital Imaging and Communications in Medicine (DICOM) standard. This uniformity allows users the unique capability to query metadata—encompassing images, annotations, and clinical attributes—across these collections. This granular control facilitates precise data subset definition or cohort creation, making the IDC an indispensable resource for researchers. IDC is a cloud-first resource. It encourages collaboration and reproducibility by utilizing Google Collaboratory Python notebooks.

The Artificial Intelligence (AI) in Medical Imaging (AIMI) initiative strives to address the ever-persistent challenge when it comes to publicly available imaging datasets: the lack of comprehensive annotations. The goal of this study, in the context of the AIMI initiative, was to curate AI-generated annotations for derived datasets from 11 distinct collections in the IDC. The image collections encompass three modalities (CT, PET, and MR), and various annotation types, as detailed in Table 1. FDG PET/CT datasets taken from The Cancer Genome Atlas (TCGA) program for Lung Adenocarcinoma (LUAD)³ and Lung Squamous Cell Carcinoma (LUSC)⁴, the Lung Cancer Diagnosis (LUNG-PET-CT-Dx)⁵, Anti-PD-1 Immunotherapy Lung⁶, the Reference Image Database to Evaluate Therapy Response PET/CT subgroup (RIDER Lung PET-CT)⁷, and the Non-Small Cell Lung Cancer (NSCLC) for Radiogenomics⁸⁻¹⁰ and the American College of Radiology Imaging Network non small cell lung cancer FDG PET (ACRIN-NSCLC-FDG-PET)^{11,12} were used for both lung and lung tumor annotations. The CTs of the previously listed lung datasets, minus ACRIN- NSCLC, were also used for the annotation of lung nodules. Breast tumor annotations were generated on FDG PET/CT breast dataset from the Quantitative Imaging Network (QIN)^{13,14}. CT annotations for kidneys, kidney tumors, and kidney cysts were generated for the Kidney Renal Clear Cell Carcinoma Collection (KIRC)¹⁵ datasets from the TCGA. MRI prostate-only annotations were generated for the ProstateX^{16,17} datasets. Liver-only annotations were generated for both CT and MRI data from the Liver Hepatocellular Carcinoma (LIHC)¹⁸ dataset of the TCGA.

Table 1: IDC collections used for AI-assisted annotations.

Collection	No. of Cases	Modality of interest (MOI)	No. of Cases w/ MOI	Annotation Task (associated modality)
TCGA-LUAD ³	560	CT, PET	68	Lungs (CT), tumors (PET/CT), and nodules (CT)
TCGA-LUSC ⁴	504	CT, PET	37	Lungs (CT), tumors (PET/CT), and nodules (CT)
LUNG-PET-CT-Dx ⁵	355	CT, PET	355	Lungs (CT), tumors (PET/CT), and nodules (CT)
Anti-PD-1-Lung ⁶	242	CT, PET	242	Lungs (CT), tumors (PET/CT), and nodules (CT)
RIDER Lung PET-CT ⁷	243	CT, PET	243	Lungs (CT), tumors (PET/CT), and nodules (CT)
NSCLC-Radiogenomics ⁸⁻¹⁰	211	CT, PET	211	Lungs (CT), tumors (PET/CT), and nodules (CT)
ACRIN-NSCLC-FDG-PET ^{11,12}	46	CT, PET	46	Lungs (CT), and tumors (PET/CT)
QIN-Breast ^{13,14}	68	CT, PET	43	Tumors (PET/CT)
TCGA-KIRC ¹⁵	537	CT	237	Kidneys (CT), tumors CT), and cysts (CT),
ProstateX ^{16,17}	346	MRI	346	Prostate (MRI)
TCGA-LIHC ¹⁸	377	CT, MRI	97	Liver (CT), Liver (MRI)

For some collections, radiology imaging data was not the main contributor of that collection^{3,4,18}. The number of cases available for each collection for AI-generated annotations was limited to the number of cases that contained the imaging region of the annotation task of interest within the modality of interest. Figure 1 shows the modality breakdown of the total number of studies within the total number of usable cases for each collection.

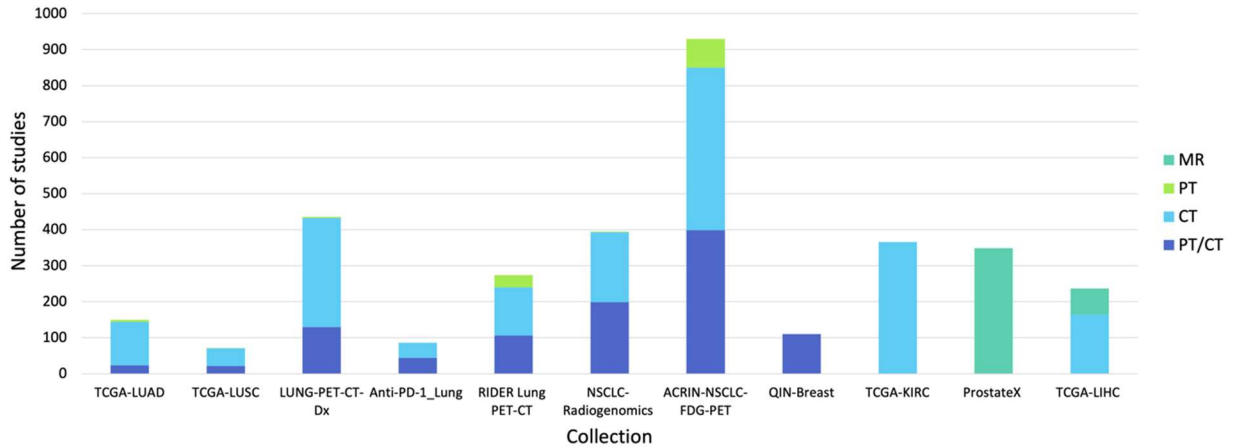


Figure 1: Modality breakdown for the total number of studies within the number of useable cases for each collection

Another component of this project was to ensure the relationship between the annotations and their represented image dataset was maintained and queryable. To achieve this, all AI-generated annotations were encoded in accordance with the Digital Imaging and Communications in Medicine (DICOM) standard¹⁹. This makes them easily accessible within the existing tools and workflows of the IDC. The annotations are also accompanied by cloud-ready analysis workflows, embodied within Google Collaboratory notebooks. These resources empower users not only to recreate the dataset but also offer practical guidance on querying, visualizing, and transforming DICOM-encoded objects into alternative representations.

In summary, this study underscores the pivotal role played by the IDC platform in ameliorating annotation deficiencies within publicly available cancer imaging datasets. Through the introduction of AI-generated annotations, we have not only enriched the utility of these collections but also exemplified the collaborative potential of AI in advancing the frontiers of cancer imaging research.

Methods

This section is structured according to the annotation type listed in Table 1 and follows the order displayed in Figure 2. Each task has its own uniquely catered methodology but follows the general workflow outline in Figure 3.

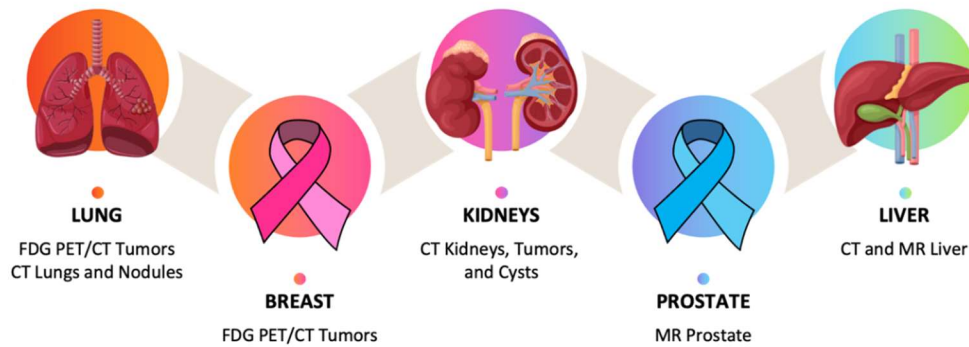


Figure 2: Illustration of the AI-generated annotation tasks and their associated modalities

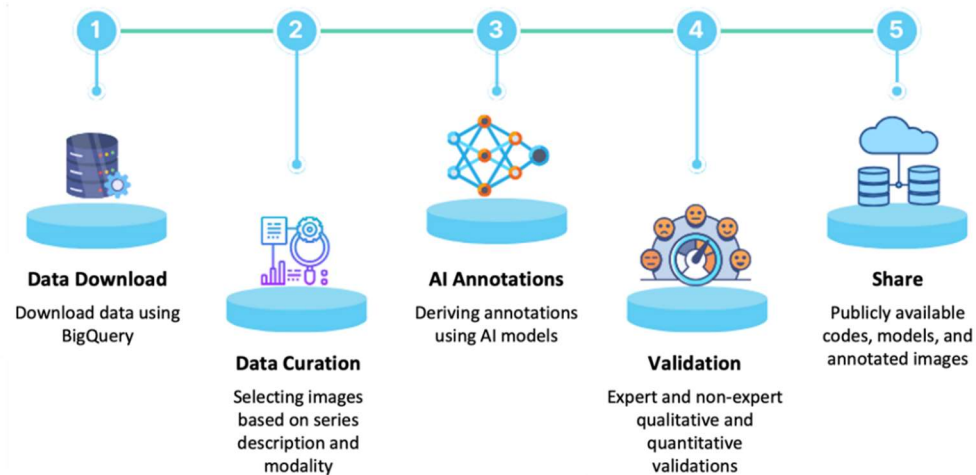


Figure 3: Annotation task workflow

All datasets were downloaded from Google Cloud Platform using BigQuery queries. Through data curation, a total of 3343 radiologic images (1118 PET, 1838 CT, and 387 MRI images) between all 11 collections (Figure 4) were identified for annotations.

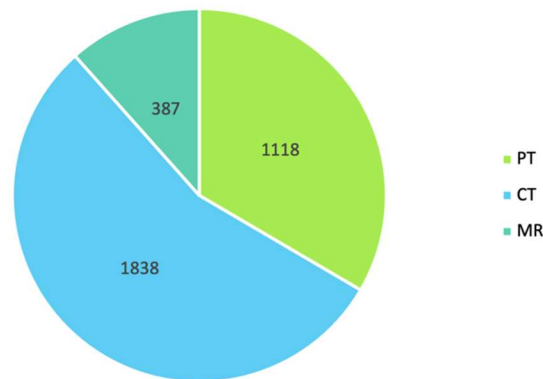


Figure 4: Distribution of the total number of images per modality of interest that could be annotated between all 11 collections.

Supervised deep learning AI models, ensembled from five-fold cross validation models using the nnU-Net²⁰ framework, were trained from a combination of the imaging data available in the IDC and additional publicly available datasets with annotations. For datasets without annotations, we relied on the output predictions generated by TotalSegmentator^{20,21}. To evaluate the quality and accuracy of the AI predictions, approximately 10% of the AI predictions were reviewed and corrected for quantifiable quality control by a Board-Certified Radiologist (expert) and an Annotation Specialist (non-expert). The Annotation Specialist has medical knowledge and passing familiarity with radiology scans but is not a certified expert.

For the 10% of data reviewed by the radiologist and annotation specialist, each of the reviewers would rate the AI prediction on a Likert Scale to assess its clinical acceptability. The Likert scale description is shown in Table 2. For cases that were not rated 'strongly agree' the reviewer would correct the ai annotation. These corrections were used to calculate the quantitative accuracy of the AI models.

The following sections go into detail about the data curation, preprocessing, analysis, and post-processing of the results steps used to develop the AI models for each specified annotation task. The code to reproduce our analysis is publicly available on GitHub.

Table 2: Likert Score description used by reviewers to assess the clinical acceptability of the AI annotations.

Likert Score	Description
Strongly agree	Use-as-is (i.e., clinically acceptable, and could be used for treatment without change)
Agree	Minor edits that are not necessary. Stylistic differences, but not clinically important. The current segmentation is acceptable.
Neither agree nor disagree	Minor edits that are necessary. Minor edits are those that the review judges can be made in less time than starting from scratch or are expected to have minimal effect on treatment outcome.
Disagree	Major edits. This category indicates that the necessary edit is required to ensure correctness, and sufficiently significant that user would prefer to start from the scratch.
Strongly disagree	Unusable. This category indicates that the quality of the automatic annotations is so bad that they are unusable.

The model outputs were converted to DICOM-SEG format and appropriate metadata was added to describe the contents and link them to the input scan. DICOM tag SegmentAlgorithmType (0062,0008) is set to “AUTOMATIC” if the segmentation is the AI output. If the segmentation is from a reviewer’s correction, the SegmentAlgorithmType is set to “SEMIAUTOMATIC”. The SegmentAlgorithmName (0062,0009) tag is set to a short name specific to the model, the specific value is given in the model overview sections below. The ContentCreatorName (0070,0084) tag and the SeriesDescription (0008,103E) tag contain the segmentation creators name, such as AI, Radiologist, or Non-expert.

FDG PET/CT Lung and Lung Tumor Annotation

IDC Collections: TCGA-LUAD, TCGA-LUSC, LUNG-PET-CT-Dx, Anti-PD-1_Lung, RIDER Lung PET-CT, NSCLC-Radiogenomics, and ACRIN-NSCLC-FDG-PET.

Data Curation: For this AI-generated annotation task imaging data must be of attenuation-corrected paired FDG-PET/CT scans of the lung/chest region. Out of the seven chosen datasets, a total of 736 paired FDG-PET/CT images matched the task criteria.

Model design and training: The AutoPET Challenge 2023 dataset^{22,23} is comprised of whole-body FDG-PET/CT data from 900 patients, encompassing 1014 studies with tumor annotations. This dataset was augmented by adding labels for the brain, bladder, kidneys, liver, stomach, spleen, lungs, and heart generated by the TotalSegmentator model. A multi-task AI model was trained using the augmented datasets¹⁸. To evaluate algorithm robustness and generalizability a held-out dataset of 150 studies was employed. Among these, 100 studies were sourced from the same hospital as the training database, while 50 were selected from a different hospital but adhered to a similar acquisition protocol. This model has achieved robust results in the final leaderboard of AutoPET challenge^{21,24}.

Preprocessing: The CT imaging data was resampled to their associated paired PET imaging data resolution.

Inference and Postprocessing: The predictions of the AI-generated FDG-avid tumor annotation model for this task were overlaid with the lung annotations provided by the TotalSegmentator model. Tumor predictions were then limited to only the predictions seen in the pulmonary and pleural regions. An example output can be seen in Figure 5.



Figure 5: Automatic segmentation of Lung (green) and FDG-avid tumor (blue) from FDG-PET/CT scans of patient RIDER-2610856938

Validation: The non-expert qualitatively assessed all 736 annotations using a Likert scale. Approximately 10% of the data (N=77) was randomly selected as a validation set. Both the non-expert and the expert Likert-scored and manually corrected the AI predictions of the validation set.

DICOM-SEG SegmentAlgorithmType: BAMF-Lung-FDG-PET-CT

CT Lung Nodule Annotation

IDC Collections: TCGA-LUAD, TCGA-LUSC, LUNG-PET-CT-Dx, Anti-PD-1_Lung, RIDER Lung PET-CT, and NSCLC-Radiogenomics

Data Curation: For this AI-generated annotation task imaging data must be CT scans of the lung/chest region that are not part of the paired attenuation-corrected FDG-PET/CT scans that were used in the previous task. Out of the six chosen datasets, a total of 433 CT scans met the task criteria.

Model design and training: The DICOM-LIDC-IDRI-Nodules dataset²⁵⁻²⁷ was used to train an AI model to annotate lung nodules. This dataset included 883 studies with annotated nodules from 875 patients. Within the dataset only nodules that were identified by all four of their radiologists (size condition: $3\text{mm} \leq \text{diameter} \leq 30\text{mm}$), were considered for AI model training for this task. The lung annotations AI model was trained on 411 and 111 lung CT data from NSCLC Radiomics^{28,29} and NSCLC Radiogenomics respectively.

Preprocessing: No additional preprocessing was used.

Inference and Postprocessing: The predictions of the AI-generated lung nodule annotation model for this task were limited to by size and regions. Only annotations that were in the pulmonary and pleural regions and had diameters between 3mm and 30mm, same as training data, were kept. An example output can be seen in Figure 6.

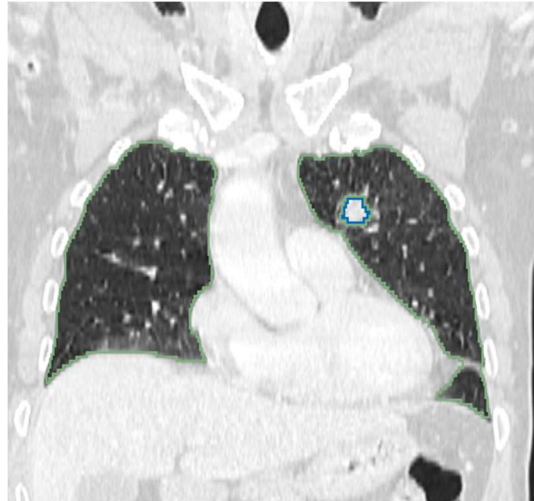


Figure 6: Automatic segmentation of Lung (green) and nodule (blue) from CT scan of patient TCGA-34-5239

Validation: The non-expert qualitatively assessed all 430 annotations using a Likert scale. Approximately 10% of the data (N=47) was randomly selected as a validation set. Both the non-expert and the expert Likert-scored and manually corrected the AI predictions of the validation set.

DICOM-SEG SegmentAlgorithmType: BAMF-Lung-CT

FDG PET/CT Breast Tumor Annotation

IDC Collections: QIN-Breast

Data Curation: For this AI-generated annotation task imaging data must be attenuation-corrected paired FDG-PET/CT. A total of 110 paired PET/CT scans met the task criteria.

Model design and training: This task used the same nnU-Net based AI model as the previous FDG-PET/CT Lung and FDG-avid Tumor task that was trained on the AutoPET Challenge 2023 dataset augmented for multitask by incorporating labels generated by TotalSegmentator.

Preprocessing: The CT imaging data was resampled to their associated paired PET imaging data resolution.

Inference and Postprocessing: The predictions of the AI-generated FDG-avid tumor annotation model for this task were overlaid with the annotations provided by the TotalSegmentator model. Tumor predictions were then limited to only the predictions seen in the breast regions. An example output can be seen in Figure 7.

Validation: The non-expert qualitatively assessed all 110 annotations using a Likert scale. Approximately 10% of the data (N=10) was randomly selected as a validation set. Both the non-expert and the expert Likert-scored and manually corrected the AI predictions of the validation set.

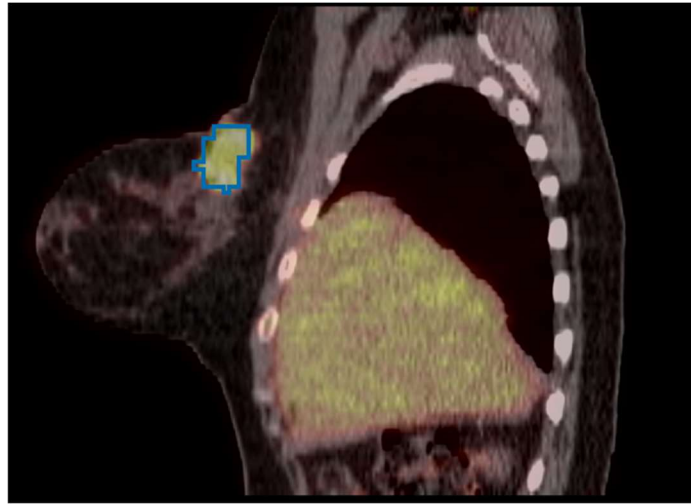


Figure 7: Automatic segmentation of FDG-avid breast tumor (blue) from FDG-PET/CT scans of patient QIN-BREAST-01-0033

DICOM-SEG SegmentAlgorithmType: BAMF-Breast-FDG-PET-CT

CT Kidneys, Tumors, and Cysts Annotation

IDC Collections: TCGA-KIRC

Data Curation: For this AI-generated annotation task imaging data was limited to contrast enhanced CT scans that contained the kidneys. A total of 156 CT scans met the task criteria.

Model design and training: The kidney tumor annotation AI model was trained to accurately delineate the kidney, tumor, and cysts. Model training was split into two stages. Stage one training used contrast CTs from the KiTS 2021 dataset³⁰ (N=489) to accurately delineate the kidney, tumor, and cysts. This trained model was then used to generate annotations for 64 cases of TCGA-KIRC collection. These annotations were then further refined by non-experts. An additional 45 cases from the TCGA-KIRC dataset were included as part of the training set for stage two training. The final trained model was used to generate annotations for all 156 cases of the TCGA-KIRC collection that met the task criteria. 43 of the annotations originated from the AI predictions of the first stage model (27 train and 16 test TCGA-KIRC cases).

Preprocessing: No additional preprocessing was used.

Inference and Postprocessing: The AI-generated annotations were limited to the two largest connected components to remove false positives. The connected components were determined from the union of the kidney, cyst, and tumor labels. An example output can be seen in Figure 8.

Validation: The non-expert qualitatively assessed all 156 kidney annotations using a Likert scale. Approximately 20% of the data (N = 39) was randomly selected as a validation set. A larger percentage of

the dataset was selected for annotation because of the heterogeneity in the collection from characteristics such as contrast phase and scan field of view. Both the non-expert and the expert Likert-scored and manually corrected the AI predictions of the validation set. Additionally, the expert provided annotations for 39 cases. This enabled a comparison between the final model's annotations and expert's annotations.

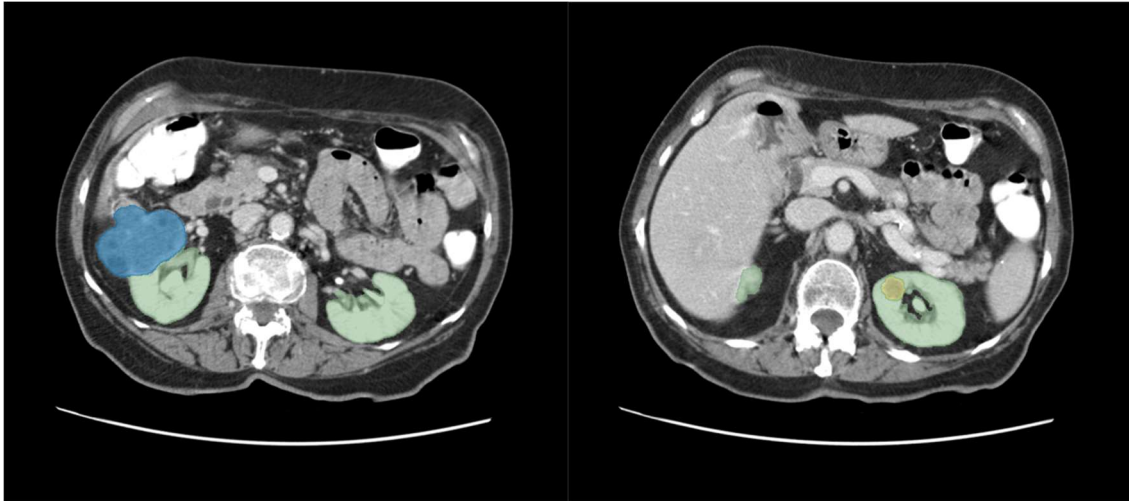


Figure 8: Automatic segmentation of kidney (green), tumor (blue), cyst (yellow) from CT scan of patient TCGA-CJ-4873

DICOM-SEG SegmentAlgorithmType: BAMF-Kidney-CT

MRI Prostate Annotation

IDC Collections: ProstateX . For this collection, the IDC has prostate annotations for 98 of the MRI scans from PROSTATEx-Seg-HiRes^{31,32} (high resolution prostate annotations, N = 66) and PROSTATEx-Seg-Zones^{33,34} (zone segmentations of the prostate, N = 32).

Data Curation: For this AI-generated annotation task imaging data was limited to T2W MRI scans that did not have any missing slices. A total of 347 MRI scans met the task criteria.

Model design and training: AI model training for this task was done in two stages. The first stage used the 98 scans of ProstateX that had associated annotations within the IDC. An additional 134 prostate annotations (PROSTATEx_masks^{35,36}) were found publicly available for ProstateX. A test/holdout validation split of 81/34 was created from the remaining 115 prostates without annotations. Along with the ProstateX dataset, additional prostate annotations for T2W MRI scans came from Prostate158³⁷ (N = 138) and ISBI-MR-Prostate-2013³⁸ (N = 69). A total of 439 T2W MRI prostate annotations were used to train the first prostate annotation AI model. This model was then used to predict 81 of the remaining unannotated scans of ProstateX and 1172 cases of the PI-CAI dataset³⁹. All ProstateX scans including the same patient were removed from the PI-CAI dataset (N = 1500) to ensure no data leakage between the two datasets. A portion of the PI-CAI dataset contained a much larger field of view than the field of view used in the training datasets. To combat the increased risk of additional off-targeting regions in the predictions the centermost segmentation (in all directions) was assumed to be the prostate and all additional regions were removed for all 1253 prostate predictions. In the second training stage a new AI model was trained using the same data as the first stage but now with the addition of the 1253 predicted annotations from the ProstateX test split and the PI-CAI dataset.

Preprocessing: No additional preprocessing was used.

Inference and Postprocessing: The AI-generated prostate annotations were limited to the largest centermost (in all directions) annotation. An example output can be seen in Figure 9.

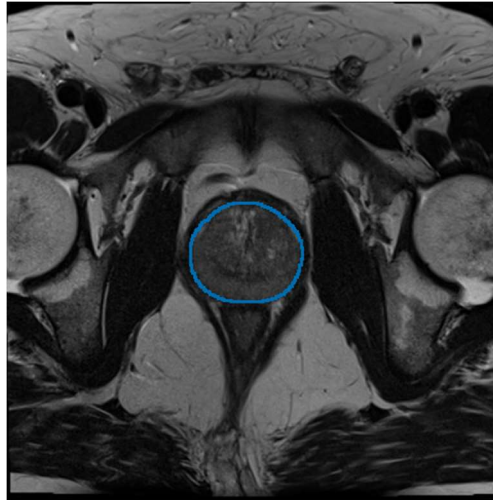


Figure 9: Automatic segmentation of prostate gland from T2 MRI scan of patient ProstateX-0336

Validation: The non-expert qualitatively assessed all 347 annotations using a Likert scale. Approximately 10% of the data (N=34) was randomly selected as a validation set. Both the non-expert and the expert Likert-scored and manually corrected the AI predictions of the validation set. Additional validation was performed by generating AI segmentation for the QIN-Prostate-Repeatability⁴⁰⁻⁴⁴, PROMISE12⁴⁵, and Medical Segmentation Decathlon⁴⁶ T2W MRI datasets.

DICOM-SEG SegmentAlgorithmType: BAMF-Prostate-MR

MRI Liver Annotation

IDC Collections: TCGA-LIHC

Data Curation: For this AI-generated annotation task imaging data was limited to T21W MRI. A total of 65 MRI scans met the task criteria.

Model design and training: 350 MRI liver annotations taken from the AMOS⁴⁷ (N=40) and DUKE Liver Dataset V2⁴⁸ (N=310) datasets were used to train an MRI liver annotation AI model.

Preprocessing: No additional preprocessing was used.

Inference and Postprocessing: The AI-generated liver annotations for were limited to the single largest connected component. An example output can be seen in Figure 10.

Validation: A non-expert qualitatively assessed all liver annotations using a Likert scale. Approximately 10% of the data (N=7) was randomly selected as a validation set. Both the non-expert and the expert Likert-scored and manually corrected the AI predictions of the validation set.

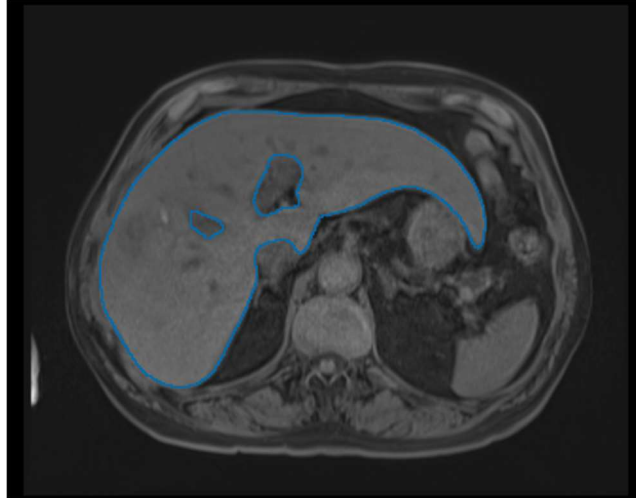


Figure 10: Automatic segmentation of the liver from T1 MRI scan of patient TCGA-G3-A7M7

DICOM-SEG SegmentAlgorithmType: BAMF-Liver-MR

CT Liver Annotation

IDC Collections: TCGA-LIHC

Data Curation: For this AI-generated annotation task imaging data was limited to CT scans of the liver region. A total of 89 CT scans met the task criteria.

Model design and training: 1565 CT liver annotations taken from the TotalSegmentator (N=1204) and FLARE21^{49,50} (N=361) datasets were used to train a CT liver annotation AI model.

Preprocessing: No additional preprocessing was used.

Inference and Postprocessing: The AI-generated liver annotations were limited to the single largest connected component. An example output can be seen in Figure 11.



Figure 11: Automatic segmentation of the liver from CT scan of patient TCGA-DD-A1EH

Validation: A non-expert qualitatively assessed all liver annotations using a Likert scale. Approximately 10% of the data (N=9) was randomly selected as a validation set. Both the non-expert and the expert Likert-scored and manually corrected the AI predictions of the validation set.

DICOM-SEG SegmentAlgorithmType: BAMF-Liver-CT

Results

The AI models were evaluated on the following series of metrics. Some of these were only applicable to a subset of the model tasks.

- Kendall's τ : measure the correlation between ordinal data, in this case, the Likert scores of the manual reviewers.
- Sørensen–Dice coefficient⁵¹ (DSC): measures the volumetric similarity between segmentations.
- Normalized Surface Dice⁵² (NSD): measures surface distance similarity. This metric takes a tolerance input that is task specific.
- 95% Hausdorff Distance: measures surface agreement. It is the distance at which 95% of the points on Surface A have a point on Surface B less than it.

For models with tumor prediction, we can measure the detection rate were:

- True positive: the predicted tumor overlaps with a ground truth tumor
- False positive: the predicted tumor does not overlap with a ground truth tumor
- False negative: the ground truth tumor does not overlap with a predicted tumor

From these, tumor detection sensitivity, false negative rate, and F1 score were calculated.

The following sections in the results are organized in the same order that was used in the methods section.

FDG PET/CT Lung and Lung Tumor Annotation

The 77 validation cases were rated by a radiologist and non-expert. Most cases were rated ‘Strongly Agree’, meaning no changes were required (Figure 12). This accounts for the good mean metrics shown in Table 3 although the lower scoring tickets cause a high standard deviation in the metrics. An important note is that there is no significant correlation as shown by Kendall’s τ . While both reviewers agreed that most of cases should be scored ‘Strongly Agree’ they disagreed on which cases those were.

Table 3: Label-wise metrics (mean (standard deviation)) between AI derived and manual corrected FDG PET/CT lungs and tumor annotations.

Segmentation Metric	Expert		Non-Expert	
	Lung	Tumor	Lung	Tumor
DSC	1.00 (0.00)	0.97 (0.11)	0.99 (0.04)	0.92 (0.20)
95% Hausdorff (mm)	0.10 (0.58)	5.83 (19.42)	1.97 (10.50)	10.00 (26.34)

Detection Accuracy	
Sensitivity	0.91
False negative rate	0.09
F1 score	0.94

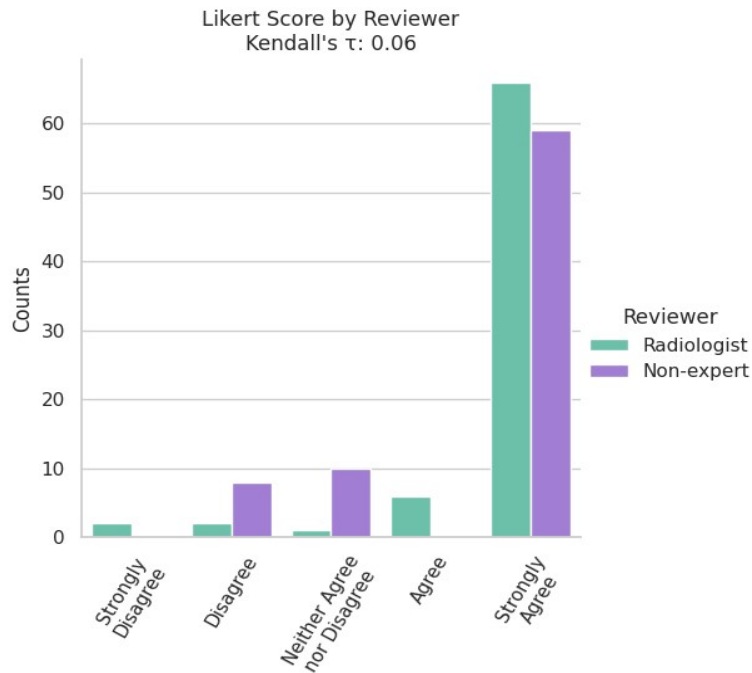


Figure 12: Counts of Likert Scores for validation set of Lung PET/CT Lung Tumor model by reviewers.

CT Lung Nodule Annotation

A validation set of 47 cases were reviewed by two radiologists. These reviewers had a moderate correlation of the Likert Scores (Kendall's $\tau = 0.42$). The variety of Likert Scores show a mix of quality output for the model, Figure 13. The model performance metrics for the validated cases are listed in Table 4. Segmentation metrics of the lung label is very high, but lower and variable for the nodule label. This lower segmentation metrics are also reflected by the low nodule detection accuracy of the model.

Table 4: Label-wise metrics (mean (standard deviation)) between AI derived and expert corrected CT lungs and nodules annotations.

Segmentation Metric	Expert 1		Expert 2	
	Lung	Nodule	Lung	Nodule
DSC	0.99 (0.02)	0.60 (0.42)	1.00 (0.00)	0.78 (0.34)
95% Hausdorff (mm)	2.34 (5.89)	56.72 (64.36)	0.30 (1.70)	26.06 (48.63)

Detection Accuracy			
Sensitivity		0.26	0.37
False negative rate		0.74	0.63
F1 score		0.41	0.54

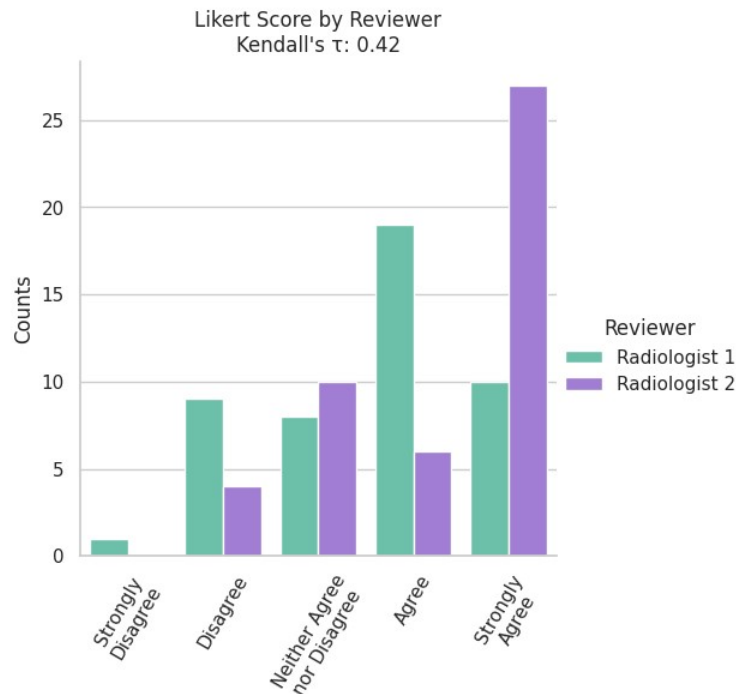


Figure 13: Counts of Likert Scores for validation set of Lung CT Lung Nodule model by reviewers.

FDG PET/CT Breast Tumor Annotation

A radiologist and non-expert reviewed the 11 validation set cases for the FDG PET/CT Breast tumor model. There was moderate correlation between reviewers Likert scores, Kendall's $\tau=0.58$, shown in Figure 14. Generally, the model did well as shown by the performance metrics in Table 5. The radiologist commented that the AI's most common failure was to include FDG-avid retropectoral lymph nodes in the breast tumor label.

Table 5: Label-wise metrics (mean (standard deviation)) between AI derived and expert corrected FDG PET/CT breast lesion annotations.

Segmentation Metric	Expert 1	Non-Expert
	Tumor	Tumor
DSC	0.80 (0.33)	0.94 (0.10)
95% Hausdorff (mm)	29.70 (33.43)	13.53 (20.00)

Detection Accuracy	
Sensitivity	0.43
False negative rate	0.57
F1 score	0.52

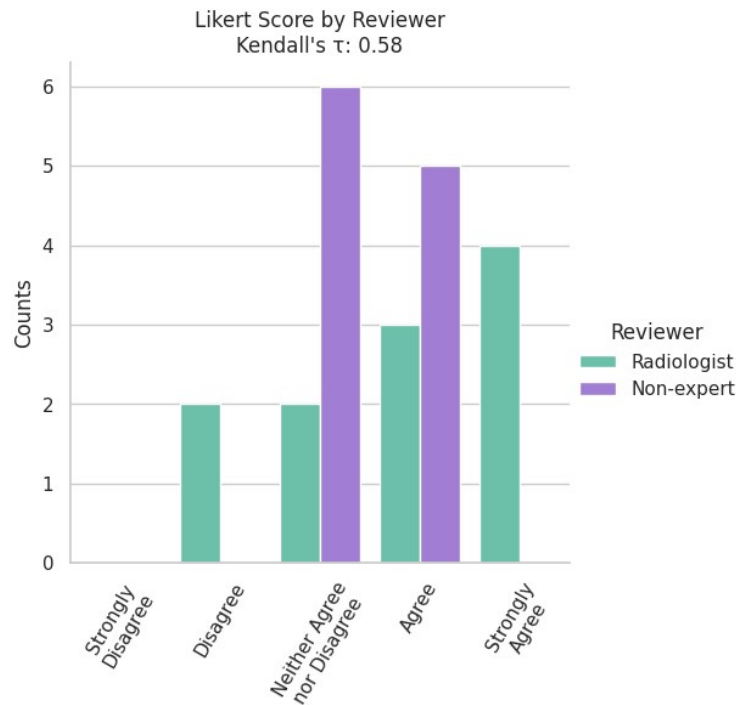


Figure 14: Counts of Likert Scores for validation set of Breast FDG-avid tumor model by reviewers.

CT Kidneys, Tumors, and Cysts Annotation

The validated set comprised 39 cases from the TCGA-KIRC IDC collection. Since the model was trained on KiTS23 data, the validation set was evaluated using the same metrics as the KiTS23 challenge. The Dice coefficient and Normalized Surface Distance were calculated for three combinations of labels: Kidney+Tumors+Cysts, Tumors+Cysts, Tumors. These metrics are shown in Table 6. Additionally, two manual reviews, a radiologist and nonexpert rated the validation set on a Likert Scale and had moderate correlation in scores as seen in Figure 15. The TCGA-KIRC dataset contains scans with a variety of contrast phases, the manual reviewers identified the contrast phase of the scan. Figure 16 shows that mean Likert scores was higher for scans in the nephrogenic and corticomedullary phase than those in the excretory phase or without contrast. The higher performance of nephrogenic and corticomedullary phase was expected because the model training set contained data from only these phases. It was interesting that scans from the Excretory phase performed as well considering the absence of this phase from the training data.

Table 6: Model performance on TCGA-KIRC data as reviewed by Radiologist and Non-expert compared to KiTS23 Challenge winner metrics on KiTS23 hidden test set. Metrics are in mean (standard deviation) format.

	DSC			NSD		
	Kidney Tumor Cyst	Tumor	Tumor Cyst	Kidney Tumor Cyst	Tumor	Tumor Cyst
KiTS23 Winner	0.96	0.76	0.79	0.91	0.62	0.64
Radiologist	0.93 (0.22)	0.88 (0.32)	0.88 (0.32)	0.91 (0.23)	0.87 (0.32)	0.87 (0.32)
Non-expert	0.99 (0.06)	0.96 (0.19)	0.96 (0.19)	0.98 (0.09)	0.95 (0.2)	0.95 (0.2)

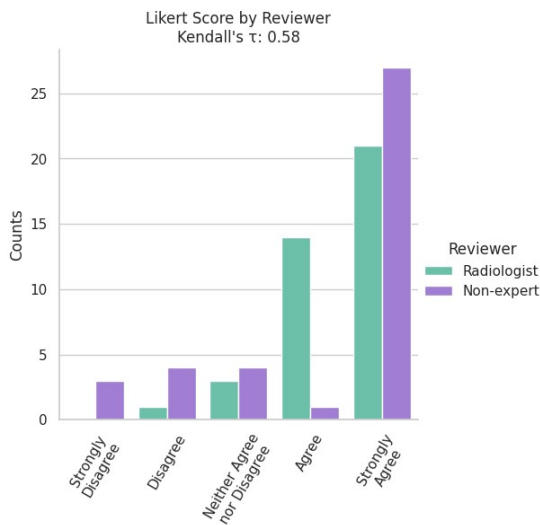


Figure 15: Counts of Likert Scores for for validation set of Lung CT Lung Nodule model by reviewers.

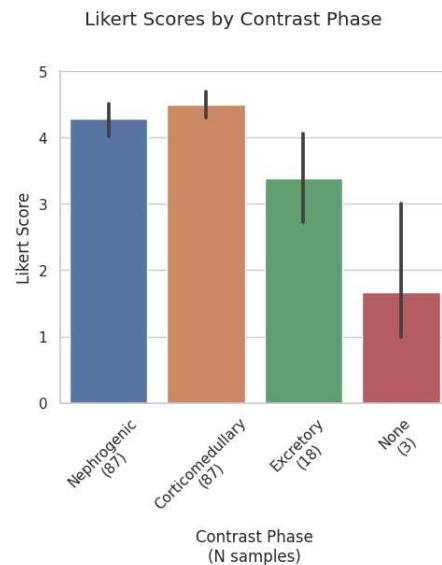


Figure 16: Mean Likert scores by contrast phase for all AI predictions from both Radiologist and non-expert.

MRI Prostate Annotation

A radiologist and non-expert reviewed the 34 validation set cases for the MRI prostate segmentation model. Both reviewers rated all 34 cases ‘Strongly Agree’, Figure 17. In addition to the 34 case validation set from ProstateX, the model’s performance was also measured against other collections with existing prostate gland segmentation, QIN-Prostate, PROMISE12, and the Medical Segmentation Decathlon (MSD). These metrics are in

Table 7, The Dice Coefficient distribution is shown in Figure 18. For this model, we used the NSD with a tolerance of 4mm as was done by the Medical Segmentation Decathlon.

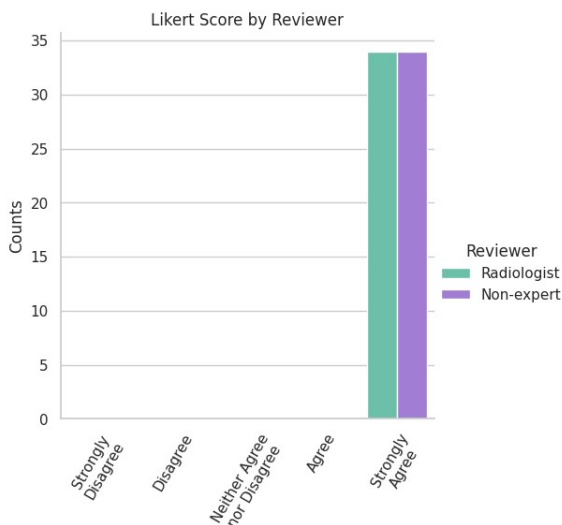


Figure 17: Counts of Likert Scores for ProstateX validation set of MRI Prostate model by reviewers.

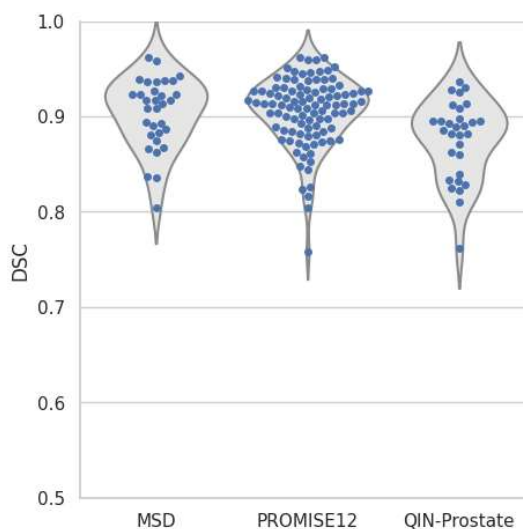


Figure 18: Dice Coefficient of AI prostate gland segmentation for Medical Segmentation Decathlon, PROMISE12, and QIN-Prostate datasets.

Table 7: Label-wise metrics (mean (standard deviation)) between AI derived and expert corrected MRI Prostate annotations and other publicly available prostate annotation datasets.

Segmentation Metric	IDC ProstateX	MSD	PROMISE12	QIN-Prostate
DSC	1.00 (0.00)	0.90 (0.04)	0.91 (0.04)	0.88 (0.04)
NSD ₄	0.00 (0.00)	0.97 (0.04)	0.97 (0.04)	0.95 (0.06)

MRI Liver Annotation

A set of 7 cases from the TCGA-LIHC collection were selected as a validation set for the MRI liver segmentation model. A radiologist and non-expert reviewed these 7 cases. The reviewers had a high correlation in the Likert scores as shown in Figure 19. Table 8 shows the DSC and NSD metrics for the validation set. A tolerance of 7mm was used for the NSD metric, same as the CT liver segmentation task from the Medical Segmentation Decathlon.

Table 8: Label-wise metrics (mean (standard deviation)) between AI derived and manually corrected MRI liver annotations.

Metric	DSC	NSD ₇
Radiologist	0.91 (0.18)	0.89 (0.20)
Non-expert	0.90 (0.15)	0.85 (0.20)

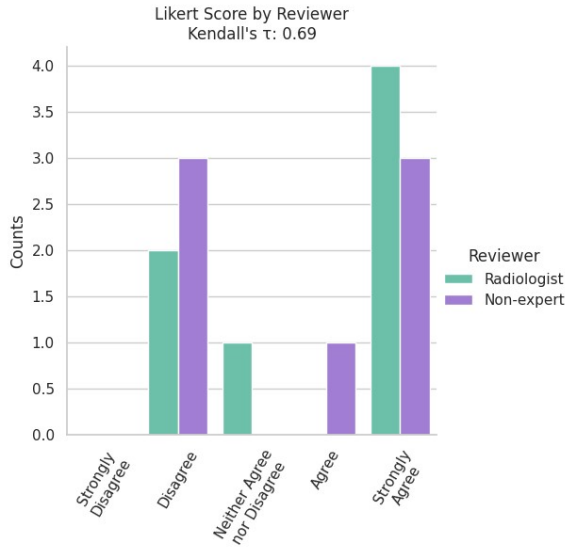


Figure 19: Reviewer Likert score comparison for MRI Liver segmentations.

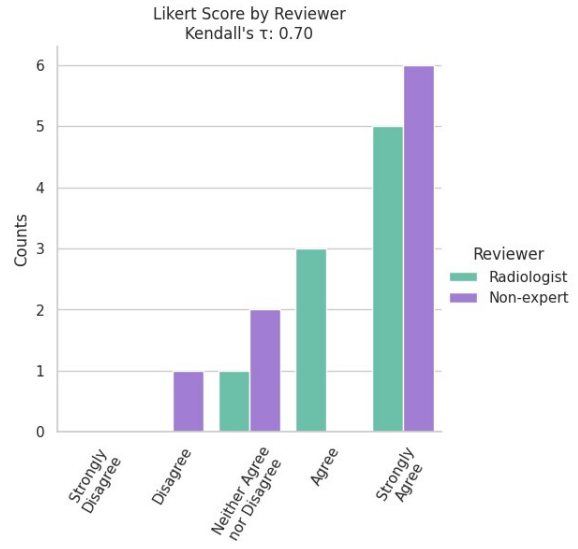


Figure 20: Counts of Likert Scores for validation set of CT liver model by reviewers.

CT Liver Annotation

The radiologist and non-expert had both rated and corrected the liver segmentation in the 9 scans of the validations set. Figure 20 shows the reviewers had high correlation of their Likert scores. This task was similar to the liver and tumor segmentation task in the Medical Segmentation Decathlon. The nnUNet architecture won that challenge. The same metrics were used to compare our model to the state of the art performance, DSC and NSD where tolerance for NSD was set to 7mm. Table 9 shows the models performance on the validation set as well as the metrics for the MSD winner on the MSD holdout set.

Table 9: Model performance on TCGA-LIHC data as reviewed by Radiologist and Non-expert compared to the Medical Segmentation Decathlon (MSD) Liver segmentation winner's metrics on the MSD hidden test set. Metrics are in mean (standard deviation) format.

Metric	DSC	NSD ₇
nnUnet (MSD)	0.95	0.98
Radiologist	0.97 (0.07)	0.96 (0.09)
Non-Expert	0.97 (0.08)	0.95 (0.11)

Conclusion

In this paper, we represent the work of AIMI producing high-quality, AI-generated annotations for selected 11 image collections from the IDC. In doing so, we employ the state-of-the-art architecture of nnUNet to train models on public datasets. The selected image collections have a diversity of image modalities and cover various body parties. Due to limited resources, a subset of the AI-generated annotations were evaluated by a board-certified Radiologist (expert) and an Annotation Specialist in order to determine the accuracy of the AI models. This manual review showed that AI models could provide accurate novel annotations to existing public datasets. Additionally, we looked at the correlation of qualitative Likert scores between an expert (radiologist) and a non-experts. Although task specific, the non-expert's scores had a moderate correlation to the expert's.

Future work could develop or refine AI models to provide a wide variety of annotations to the many collections in the IDC. Supplemental work might also look for programmatic ways to assess AI annotation quality in relation to the manual scoring performed in this project.

Data Availability

The reviewers scoring and comments, as well as DICOM Segmentation objects for the AI predictions and reviewer's corrections are available at <https://zenodo.org/doi/10.5281/zenodo.8345959>

The model weights are also available on zenodo.org and the notebook code to reproduce the analysis can be found on GitHub. The URLs are given in Table 10.

Table 10: URLs for model weights and analysis code

Task	Model Weights	Notebook Code
FDG PET/CT Lung and Lung Tumor Annotation	https://doi.org/10.5281/zenodo.8290054	https://github.com/bamf-health/aimi-lung-pet-ct
CT Lung Nodule Annotation	https://doi.org/10.5281/zenodo.8290146 https://zenodo.org/record/8290169	https://github.com/bamf-health/aimi-lung-ct
FDG PET/CT Breast Tumor Annotation	https://doi.org/10.5281/zenodo.8290054	https://github.com/bamf-health/aimi-breast-pet-ct
CT Kidneys, Tumors, and Cysts Annotation	https://doi.org/10.5281/zenodo.8277845	https://github.com/bamf-health/aimi-kidney-ct
MRI Prostate Annotation	https://doi.org/10.5281/zenodo.8290092	https://github.com/bamf-health/aimi-prostate-mr
MRI Liver Annotation	https://doi.org/10.5281/zenodo.8290123	https://github.com/bamf-health/aimi-liver-mr
CT Liver Annotation	https://doi.org/10.5281/zenodo.8270230	https://github.com/bamf-health/aimi-liver-ct

Acknowledgements

This project has been funded in whole or in part with Federal funds from the National Cancer Institute, National Institutes of Health, under Contract No. 75N91019D00024, Task Order No. 75N91020F0003. The

content of this publication does not necessarily reflect the views or policies of the Department of Health and Human Services, nor does mention of trade names, commercial products or organizations imply endorsement by the U.S. Government.

The results published here are in whole or part based upon data generated by the TCGA Research Network: <http://cancergenome.nih.gov/>

Sharing of the QIN-Breast collection is funded in part or whole by the NCI grand U01 CA142565

Sharing of the QIN-Prostate-Repeatability collection is funded in part or whole by the NCI grand U01 CA151261

Conflict of Interests

There are no conflicts of interest.

References

1. Fedorov, A. *et al.* NCI imaging data commons. *Cancer Res* **81**, 4188 (2021).
2. Clark, K. *et al.* The Cancer Imaging Archive (TCIA): Maintaining and Operating a Public Information Repository. doi:10.1007/s10278-013-9622-7.
3. Albertina, B. *et al.* The Cancer Genome Atlas Lung Adenocarcinoma Collection (TCGA-LUAD) (Version 4) [Data set]. *The Cancer Imaging Archive* <https://doi.org/10.7937/K9/TCIA.2016.JGNIHEP5> (2016).
4. Kirk, S. *et al.* The Cancer Genome Atlas Lung Squamous Cell Carcinoma Collection (TCGA-LUSC) (Version 4) [Data set]. *The Cancer Imaging Archive* <https://doi.org/10.7937/K9/TCIA.2016.TYGKFKFMQ> (2016).
5. Li, P. *et al.* A Large-Scale CT and PET/CT Dataset for Lung Cancer Diagnosis (Lung-PET-CT-Dx) [Data set]. *The Cancer Imaging Archive* <https://doi.org/10.7937/TCIA.2020.NNC2-0461> (2020).
6. Madhavi, P., Patel, S. & Tsao, A. S. Data from Anti-PD-1 Immunotherapy Lung [Data set]. *The Cancer Imaging Archive* <https://doi.org/10.7937/tcia.2019.zjjwb9ip> (2019).
7. Muzi, P., Wanner, M. & Kinahan, P. Data From RIDER Lung PET-CT. *The Cancer Imaging Archive Preprint* at <https://doi.org/10.7937/k9/tcia.2015.ofip7tvm> (2015).
8. Gevaert, O. *et al.* Non–Small Cell Lung Cancer: Identifying Prognostic Imaging Biomarkers by Leveraging Public Gene Expression Microarray Data—Methods and Preliminary Results. *Radiology* **264**, 387–396 (2012).
9. Bakr, S. *et al.* Data for NSCLC Radiogenomics (Version 4) [Data set]. *The Cancer Imaging Archive* (2017).
10. Bakr, S. *et al.* A radiogenomic dataset of non-small cell lung cancer. *Sci Data* **5**, 180202 (2018).
11. Kinahan, P., Muzi, M., Bialecki, B., Herman, B. & Coombs, L. Data from the ACRIN 6668 Trial NSCLC-FDG-PET (Version 2) [Data set]. *The Cancer Imaging Archive* <https://doi.org/10.7937/tcia.2019.30ilqfcl> (2019).
12. Machtay, M. *et al.* Prediction of Survival by [18F]Fluorodeoxyglucose Positron Emission Tomography in Patients With Locally Advanced Non–Small-Cell Lung Cancer Undergoing Definitive Chemoradiation Therapy: Results of the ACRIN 6668/RTOG 0235 Trial. *Journal of Clinical Oncology* **31**, 3823–3830 (2013).
13. Li, X. *et al.* Data From QIN-Breast (Version 2) [Data set]. *The Cancer Imaging Archive* <https://doi.org/10.7937/K9/TCIA.2016.21JUEBH0> (2016).
14. Li, X. *et al.* Multiparametric Magnetic Resonance Imaging for Predicting Pathological Response After the First Cycle of Neoadjuvant Chemotherapy in Breast Cancer. *Invest Radiol* **50**, 195–204 (2015).

15. Akin, O. *et al.* The Cancer Genome Atlas Kidney Renal Clear Cell Carcinoma Collection (TCGA-KIRC) (Version 3) [Data set]. *The Cancer Imaging Archive* <https://doi.org/10.7937/K9/TCIA.2016.V6PBVTDR> (2016).
16. Litjens, J. B., Debats, O., Barentsz, J., Karssemeijer, N. & Huisman, H. SPIE-AAPM-NCI PROSTATEx Challenges. *The Cancer Imaging Archive* <https://doi.org/10.7937/K9TCIA.2017.MURS5CL> (2017).
17. Litjens, G., Debats, O., Barentsz, J., Karssemeijer, N. & Huisman, H. Computer-Aided Detection of Prostate Cancer in MRI. *IEEE Trans Med Imaging* **33**, 1083–1092 (2014).
18. Erickson, B. J. *et al.* The Cancer Genome Atlas Liver Hepatocellular Carcinoma Collection (TCGA-LIHC) (Version 5) [Data set]. *The Cancer Imaging Archive* <https://doi.org/10.7937/K9/TCIA.2016.IMMQW8UQ> (2016).
19. Digital Imaging and Communications in Medicine (DICOM). in *NEMA Publications PS 3.1-PS 3.12*. (The National Electrical Manufacturers Association, 1992).
20. Isensee, F., Jaeger, P. F., Kohl, S. A. A., Petersen, J. & Maier-Hein, K. H. nnU-Net: a self-configuring method for deep learning-based biomedical image segmentation. *Nature Methods* **2020 18:2 18**, 203–211 (2020).
21. Wasserthal, J. *et al.* TotalSegmentator: Robust Segmentation of 104 Anatomic Structures in CT Images. *Radiol Artif Intell* **5**, (2023).
22. Gatidis, S. & Kuestner, T. A whole-body FDG-PET/CT dataset with manually annotated tumor lesions (FDG-PET-CT-Lesions) [Dataset]. *The Cancer Imaging Archive* <https://doi.org/10.7937/gkr0-xv29> (2022).
23. Gatidis, S. *et al.* A whole-body FDG-PET/CT Dataset with manually annotated Tumor Lesions. *Sci Data* **9**, 601 (2022).
24. Murugesan, G. K. *et al.* Automatic Whole Body FDG PET/CT Lesion Segmentation using Residual UNet and Adaptive Ensemble. *bioRxiv* 2023.02.06.525233 (2023) doi:10.1101/2023.02.06.525233.
25. Fedorov, A. *et al.* Standardized representation of the TCIA LIDC-IDRI annotations using DICOM. *The Cancer Imaging Archive* <https://doi.org/10.7937/TCIA.2018.h7umfurq> (2018).
26. Armato, S. G. *et al.* The Lung Image Database Consortium (LIDC) and Image Database Resource Initiative (IDRI): A completed reference database of lung nodules on CT scans. *Med Phys* **38**, 915–931 (2011).
27. Fedorov, A. *et al.* DICOM re-encoding of volumetrically annotated Lung Imaging Database Consortium (LIDC) nodules. *Med Phys* **47**, 5953–5965 (2020).
28. Aerts, H. J. W. L. *et al.* Data From NSCLC-Radiomics (version 4) [Data set]. *The Cancer Imaging Archive*. <https://doi.org/10.7937/K9/TCIA.2015.PFOM9REI> (2014).
29. Aerts, H. J. W. L. *et al.* Decoding tumour phenotype by noninvasive imaging using a quantitative radiomics approach. *Nat Commun* **5**, 4006 (2014).

30. Heller, N. *et al.* The KiTS21 Challenge: Automatic segmentation of kidneys, renal tumors, and renal cysts in corticomedullary-phase CT. Preprint at (2023).
31. Schindele, D. *et al.* High Resolution Prostate Segmentations for the ProstateX-Challenge [Data set]. *The Cancer Imaging Archive* <https://doi.org/10.7937/TCIA.2019.DEG7ZG1U> (2020).
32. Meyer, A. *et al.* Anisotropic 3D Multi-Stream CNN for Accurate Prostate Segmentation from Multi-Planar MRI. *Comput Methods Programs Biomed* **200**, 105821 (2021).
33. Meyer, A. *et al.* PROSTATEx Zone Segmentations [Data set]. *The Cancer Imaging Archive* <https://doi.org/10.7937/TCIA.NBB4-4655> (2020).
34. Meyer, A. *et al.* Towards Patient-Individual PI-Rads v2 Sector Map: Cnn for Automatic Segmentation of Prostatic Zones From T2-Weighted MRI. in *2019 IEEE 16th International Symposium on Biomedical Imaging (ISBI 2019)* 696–700 (IEEE, 2019). doi:10.1109/ISBI.2019.8759572.
35. Cuocolo, R., Stanzione, A., Castaldo, A., De Lucia, D. R. & Imbriaco, M. Quality control and whole-gland, zonal and lesion annotations for the PROSTATEx challenge public dataset. *Eur J Radiol* **138**, 109647 (2021).
36. Cuocolo, R. *et al.* Deep Learning Whole-Gland and Zonal Prostate Segmentation on a Public MRI Dataset. *Journal of Magnetic Resonance Imaging* **54**, 452–459 (2021).
37. Bressemer, K., Adams, L. & Engel, G. Prostate158 - Training data (version 1) [Data set]. In *Computers in Biology and Medicine* **148**, 105817 (2022).
38. Bloch N *et al.* NCI-ISBI 2013 Challenge: Automated Segmentation of Prostate Structures. *The Cancer Imaging Archive* <http://doi.org/10.7937/K9/TCIA.2015.zF0vIOPv> (2015).
39. Saha, A. *et al.* The PI-CAI Challenge: Public Training and Development Dataset. (2022) doi:10.5281/ZENODO.6624726.
40. Fedorov, A. *et al.* Data From QIN-PROSTATE-Repeatability. *The Cancer Imaging Archive* Preprint at <https://doi.org/10.7937/K9/TCIA.2018.MR1CKGND> (2018).
41. Fedorov, A., Vangel, M. G., Tempany, C. M. & Fennessy, F. M. Multiparametric Magnetic Resonance Imaging of the Prostate. *Invest Radiol* **52**, 538–546 (2017).
42. Fedorov, A. *et al.* An annotated test-retest collection of prostate multiparametric MRI. *Sci Data* **5**, 180281 (2018).
43. Peled, S. *et al.* Selection of Fitting Model and Arterial Input Function for Repeatability in Dynamic Contrast-Enhanced Prostate MRI. *Acad Radiol* **26**, e241–e251 (2019).
44. Schwier, M. *et al.* Repeatability of Multiparametric Prostate MRI Radiomics Features. *Sci Rep* **9**, 9441 (2019).
45. Litjens, G. *et al.* PROMISE12: Data from the MICCAI Grand Challenge: Prostate MR Image Segmentation 2012. (2023) doi:10.5281/ZENODO.8026660.

46. Antonelli, M. *et al.* The Medical Segmentation Decathlon. *Nat Commun* **13**, 4128 (2022).
47. Ji, Y. *et al.* AMOS: A Large-Scale Abdominal Multi-Organ Benchmark for Versatile Medical Image Segmentation. (2022).
48. Macdonald, J. A. *et al.* Duke Liver Dataset: A Publicly Available Liver MRI Dataset with Liver Segmentation Masks and Series Labels. <https://doi.org/10.1148/ryai.220275> **5**, (2023).
49. Ma, J. *et al.* Fast and Low-GPU-memory abdomen CT organ segmentation: The FLARE challenge. *Med Image Anal* **82**, 102616 (2022).
50. Ma, J. MICCAI 2021 FLARE Challenge Dataset. Preprint at <https://doi.org/10.1109/TPAMI.2021.3100536> (2022).
51. Dice, L. R. Measures of the Amount of Ecologic Association Between Species. *Ecology* **26**, 297–302 (1945).
52. Nikolov, S. *et al.* Clinically Applicable Segmentation of Head and Neck Anatomy for Radiotherapy: Deep Learning Algorithm Development and Validation Study. *J Med Internet Res* **23**, e26151 (2021).